AIAA JOURNAL
Vol. 36, No. 6, June 1998

Experimental Validation of Lifting Surface Theory for Rotor–Stator Interaction Noise Generation

Pieter Sijtsma,* Edward R. Rademaker,* and Johan B. H. M. Schulten†
National Aerospace Laboratory NLR, 8300 AD Emmeloord, The Netherlands

An important element in the National Aerospace Laboratory NLR prediction model for rotor–stator interaction noise is the unsteady lifting surface theory for a rotating blade row. To validate this lifting surface theory, a wind-tunnel experiment has been carried out using a through-flow nacelle with a hub, a 16-bladed rotor, and an 18-vane stator. Two mechanisms of sound generation were recognized. As usual in rotor–stator configurations, sound was produced by interaction of rotor viscous wakes with the downstream stator vanes. In addition, due to the small gap between rotor and stator, sound was generated by interaction of the stator vanes, with flow distortions caused by the thickness of the rotor blades and vice versa. Trip wires were attached to blades and vanes to simulate high-Reynolds-number flow. Unsteady pressures were measured on a stator vane, on a rotor blade, and in the inlet. Experiment and theory are briefly described, and results from both are compared. For most of the measured cases, the agreement is good.

Nomenclature

B	= number of rotor blades
C_p	= pressure coefficient
h	= hub radius
i	= imaginary unit
J_m	= mth-order Bessel function of the first kind
k	= circumferential mode number (incident field)
M	= Mach number of axial flow
m	= circumferential mode number (resulting field)
p	= pressure disturbance
r	= radial coordinate
$U_{m\mu}$	= radial eigenfunction
V	= number of stator vanes
$\boldsymbol{v}$	= disturbance velocity
x	= axial coordinate
Y_m	= mth-order Bessel function of the second kind
α	= axial wave number
β	= $(1 - M^2)^{1/2}$
ε	= eigenvalue
θ	= circumferential coordinate
μ	= radial mode number
Ω	= circumferential tip Mach number
ω	= frequency (dimensionless)
ω_k	= frequency of incident field
ω_l	= frequency in blade-fixed frame
ω_m	= frequency of resulting field

I. Introduction

In the development of turbofan engines for civil aircraft, there is a trend toward higher and higher bypass ratios. New engines have lower fan speeds and are quieter than the older models. A low fan speed is important because an isolated fan does not produce sound when it operates at subsonic relative (helical) tip speed. Then, the interaction of the fan (rotor) with the downstream stator is the most important noise-generating mechanism.

Rotor–stator interaction is a complicated process. Both rotor and stator generate flow distortions, thus inducing unsteady loading on each other. Consequently, both rotor and stator act as sound sources. Sound waves are generated at the rotor blade-passing frequency (BPF) and its higher harmonics. Their circumferential mode numbers are linear combinations of the number of rotor blades and the number of stator vanes.[1] Usually, these numbers are chosen such that the BPF is cut off.

To describe the several aspects of rotor–stator interaction and to predict the resulting noise, a three-dimensional theoretical model was developed, based on lifting surface theory.[2] In this model a uniform main flow is assumed, compared to which the distortions caused by rotor and stator are small. Additionally, computer programs were written to quantify the noise sources. The theory can be used to optimize the shielding effect of a rotor.[3]

Part of the theory was validated in 1989 by Schulten[4] using an experiment by Zandbergen[5] in the National Aerospace Laboratory NLR low-speed wind tunnel. A row of 18 stator vanes was installed in a through-flow nacelle, and a set of 16 rotating rods was used to generate viscous wakes. The unsteady wake velocities were measured, and with this measured incident field, the unsteady stator loading was numerically predicted. On an instrumented stator vane, the unsteady pressure was measured and compared with numerical results. Although the velocity distortions were rather high (up to 20% of the main velocity), the experimental and numerical results agreed very well.

Measurements of rotor-wake-induced unsteady stator loading using vane-mounted transducers have been carried out by Fleeter et al.[6] Their experiment was set up to investigate the applicability of a two-dimensional theory for the interaction of gusts with vane rows.[7] The hub/tip ratio was high (0.8) to diminish three-dimensional effects. Good agreement between measurements and theory also was reported.

In 1995, a new experiment with the NLR fan model was carried out, this time with the rods replaced by an actual, unloaded rotor. Trip wires were attached to both sides of each rotor blade and each stator vane to fix the transition from laminar to turbulent boundary-layer flow. One of the rotor blades was instrumented at midspan to measure the local unsteady loading. Further, the resulting sound in the intake was measured using an annular array of transducers mounted in the duct wall. The axial gap between rotor and stator was small, and therefore the primary noise sources were not only the viscous wakes from the rotor blades but also the flow distortions caused by the thickness of rotor blades and stator vanes. The goal of this new experiment was to validate the lifting surface theory for a rotating blade row so that the theory could be used with some confidence to include the effect of rotor shielding. In this paper the comparison of experimental and theoretical results is discussed.

This paper is organized as follows. In Sec. II the physics of rotor–stator interaction noise generation is reviewed. Section III briefly outlines the theoretical modeling, and Sec. IV gives a description of

Presented as Paper 96-1744 at the AIAA/CEAS 2nd Aeroacoustics Conference, State College, PA, May 6–8, 1996; received March 18, 1997; revision received Dec. 10, 1997; accepted for publication Jan. 18, 1998.

*Research Engineer, Aeroacoustics Department.
†Senior Research Engineer, Aeroacoustics Department. Senior Member AIAA.

the experiment. Section V describes the validation, and the conclusions are stated in Sec. VI.

II. Rotor–Stator Interaction

As in Ref. 2, we consider an annular flow duct with a uniform, subsonic main flow of Mach number M. The flow is assumed to be inviscid and isentropic. Noise is induced by flow distortions, which are supposed to be small. In this section a brief discussion is given on flow distortions, on the interaction of a flow distortion with a blade row, and on the features of rotor–stator interaction noise. The physical properties that we consider are made dimensionless using the duct radius, the ambient density, and the ambient speed of sound. Cylindrical coordinates (x, r, θ) are defined in the duct.

Flow Distortions

Under the mentioned restrictions, the governing equations for the dimensionless disturbance pressure p and velocity $\boldsymbol{v}$ are

$$\frac{\mathrm{D}p}{\mathrm{D}t} + \nabla \cdot \boldsymbol{v} = 0 \tag{1}$$

$$\frac{\mathrm{D}\boldsymbol{v}}{\mathrm{D}t} + \nabla p = 0 \tag{2}$$

where

$$\frac{\mathrm{D}}{\mathrm{D}t} = \frac{\partial}{\partial t} + M\frac{\partial}{\partial x} \tag{3}$$

Two classes of solutions can be distinguished. The first class consists of solutions with $p = 0$. Possible solutions for $\boldsymbol{v}$ can be written as

$$\boldsymbol{v} = \nabla \times \boldsymbol{\Phi}[t - (x/M), \theta, r] \tag{4}$$

where $\nabla\times$ is the curl operator. For a single dimensionless frequency ω and circumferential mode number m, Eq. (4) reduces to

$$\boldsymbol{v} = \nabla \times [\exp(i\{\omega[t - (x/M)] - m\theta\})\boldsymbol{\Phi}(r)] \tag{5}$$

where i is the imaginary unit. These solutions are called vortical waves. Vortical waves always are convected downstream from the source.

The second class consists of solutions with nonzero p governed by the convective Helmholtz equation

$$\frac{\mathrm{D}^2 p}{\mathrm{D}t^2} - \nabla^2 p = 0 \tag{6}$$

Solutions (modes) with specified ω and m have the form

$$p(x, r, \theta, t) = A \exp[i(\omega t + \alpha x - m\theta)]U_{m\mu}(r) \tag{7}$$

where A is the modal amplitude and $U_{m\mu}$ is a radial eigenfunction satisfying the hard wall boundary condition at $r = h$ (hub) and $r = 1$ (shroud). The axial wave numbers α follow from the dispersion relation

$$\alpha = (1/\beta^2)\left[M\omega \pm (\omega^2 - \beta^2\varepsilon^2)^{\frac{1}{2}}\right] \tag{8}$$

Here $\beta^2 = 1 - M^2$ and ε is a solution of

$$J'_m(\varepsilon)Y'_m(\varepsilon h) - Y'_m(\varepsilon)J'_m(\varepsilon h) = 0 \tag{9}$$

The unsteady velocity $\boldsymbol{v}$ associated with Eq. (7) follows from Eq. (2) and has the form

$$\boldsymbol{v} = \frac{-A}{i(\omega + M\alpha)} \begin{bmatrix} i\alpha \\ \partial/\partial r \\ -im/r \end{bmatrix} \exp[i(\omega t + \alpha x - m\theta)]U_{m\mu}(r) \tag{10}$$

These solutions are acoustic waves. Acoustic waves propagate both upstream and downstream from the source.

Within the acoustic waves, we can identify propagating or cuton modes and nonpropagating or cutoff modes. Cuton modes are modes for which α is real ($\omega^2 \geq \beta^2\varepsilon^2$); cutoff modes are modes for which α has a nonzero imaginary part ($\omega^2 < \beta^2\varepsilon^2$). Resonance occurs when $\omega^2 = \beta^2\varepsilon^2$.

In fact, vortical waves and acoustic waves are eigensolutions of the linearized Euler equations in the presence of a uniform main flow, as clearly explained by Tam and Webb.[8]

Interaction Mechanism

Suppose that the main flow is disturbed by an unsteady vortical or acoustic wave of frequency ω_k and circumferential mode number k, i.e., the disturbance velocity has the form

$$\boldsymbol{v}(x, r, \theta, t) = \boldsymbol{v}_k(x, r) \exp[i(\omega_k t - k\theta)] \tag{11}$$

Then the blades of a blade row that rotates with tangential tip Mach number Ω experience a flow distortion of frequency

$$\omega_l = \omega_k - k\Omega \tag{12}$$

The experienced frequency ω_l is different from the incident frequency ω_k because ω_l is the frequency in a rotating frame of reference. As a reaction, unsteady pressure jumps are induced across the blade surfaces with the same frequency ω_l. This unsteady loading, or fluctuating lift, has the property that the component normal to the blade surfaces of its induced velocity field is opposite to the normal component of the incident velocity so that the total flowfield is tangential. Consequently, the blade row acts as a source for a sequence of acoustic waves with frequencies

$$\omega_m = \omega_k + nB\Omega, \qquad n = \ldots, -2, -1, 0, 1, 2, \ldots \tag{13}$$

The corresponding circumferential mode numbers are

$$m = k + nB \tag{14}$$

Interaction Noise

Consider a rotor with B blades, rotating with tip Mach number Ω, and a downstream stator with vane number V. Flow distortions that induce rotor–stator interaction noise are 1) the rotor-bound potential field caused by steady loading of the rotor blades (acoustic modes), 2) the stator-bound potential field caused by steady loading of the stator vanes (nonpropagating acoustic modes of zero frequency), 3) the rotor-bound potential field caused by thickness of the rotor blades (acoustic modes), 4) the stator-bound potential field caused by thickness of the stator vanes (nonpropagating acoustic modes of zero frequency), 5) the downstream convected vortical wakes caused by steady loading of the rotor blades, and 6) the downstream convected viscous wakes that are caused by the boundary-layer development at the rotor blade surfaces.

The distortions caused by blade/vane thickness (distortions 3 and 4) quickly diminish for increasing rotor–stator gaps. In a full-size turbofan they are negligible. Further, the acoustic distortions 1 and 2 are usually weak compared with the convective distortions 5 and 6.

The viscous wakes (distortion 6) do not fall within the inviscid approach, but a well-developed turbulent wake can be modeled by a shear layer,[9] in other words, by a vortical wake. The rotor-induced distortions (1, 3, 5, and 6) have frequencies $n_1 B\Omega$ and mode numbers $n_1 B$. These distortions interact with the stator, where unsteady loading is induced at frequencies $n_1 B\Omega$. Consequently, acoustic waves are produced with frequencies $n_1 B\Omega$ and mode numbers $n_1 B - n_2 V$. These waves impinge on the rotor, inducing unsteady loading there at frequencies $n_2 V\Omega$, as follows from Eq. (12). Then, the rotor acts as a source for acoustic waves with frequencies $(n_1 + n_3)B\Omega$ and mode numbers $(n_1 + n_3)B - n_2 V$. Thus, each harmonic n_1 of the unsteady loading on the stator vanes contributes to each harmonic $(n_1 + n_3)$ in front of the rotor.

Furthermore, the stator-induced distortions (2 and 4) have zero frequency and mode numbers $-n_2 V$. By interaction at the rotor, where unsteady loading at frequencies $n_2 V\Omega$ is induced, acoustic waves are produced with frequencies $n_3 B\Omega$ and mode numbers $n_3 B - n_2 V$.

It is noted here that the stator vanes and the rotor blades experience unsteady loading at different frequencies. At the stator vanes, the loading is at multiples of the rotor blade-passing frequency $B\Omega$, whereas at the rotor blades the loading is at multiples of the stator vane-passing frequency $V\Omega$.

Acoustic waves, generated at the rotor, impinge on the stator, where new acoustic waves are formed. These diffracted waves interact with the rotor, where again new acoustic waves are formed, and so on. The process of interaction continually repeats itself. However, the newly created waves become weaker at each iteration step.

Thus, to obtain the sound in front of the rotor, many components have to be summed: 1) sound generated at the stator by the interaction with rotor-induced flow distortions, 2) sound generated at the rotor by the interaction with stator-induced flow distortions, 3) sound generated at the rotor by the interaction with acoustic waves from the stator (rotor diffraction), and 4) sound generated by multiple diffraction on stator and rotor.

III. Theoretical Model

The lifting surface theory to be validated is described in Ref. 2. Herein, the flow is inviscid and isentropic. A uniform subsonic main flow is assumed, on which small distortions governed by Eqs. (1) and (2) are superposed. As described in Sec. II, vortical and acoustic waves can be distinguished.

The blades of a blade row (rotor or stator) are modeled by lifting surfaces, i.e., infinitely thin reference surfaces across which steady and unsteady pressure discontinuities are allowed. The blade thickness is modeled by velocity monopoles located at the reference surfaces. Viscous wakes are modeled using Schlichting's turbulent wake model.[9] The lifting surface model is consistent with the linearized theory. Linearized theory fails when the blades are too heavily loaded or too thick.

The most difficult part of the theory is to obtain the pressure jump across the reference surface, given an incident field. The pressure jump or loading Δp satisfies a Fredholm integral equation of the first kind, symbolically written

$$\int K(z,\zeta)\Delta p(\zeta)\,\mathrm{d}\zeta = f(z) \tag{15}$$

When unsteady loading is considered, the right-hand side f follows from the incident field. For the steady loading problem, f depends also on angle of incidence, blade camber, and blade thickness. The kernel K depends only on the fan operating condition.

The unknown loading Δp is solved from Eq. (15) by expressing it in a series of suitably chosen basis functions and by applying a Galerkin projection. Then the unknown pressure coefficients can be solved from a linear system of equations

$$L\boldsymbol{P} = \boldsymbol{R} \tag{16}$$

where L is a matrix of influence coefficients, $\boldsymbol{P}$ is a vector of pressure coefficients, and $\boldsymbol{R}$ is a vector that follows from the incident field.

Based on this lifting surface theory, computer programs were written. The use of these programs is restricted to unswept blades: the leading and the trailing edges are assumed to be in planes perpendicular to the axis. In other words, the x coordinates of the edges do not vary in the spanwise direction. With this geometrical restriction, separation of variables can be applied, and the computational effort is much less than it would be for more general blade shapes. For swept blades, an alternative approach is given in Ref. 10.

Computations are carried out at a prescribed accuracy. However, a higher accuracy of the influence coefficients usually leads to sharp increases in computing time. A practical limit to the accuracy is about 0.1%. The computed results shown here have an accuracy of 1%.

IV. Experimental Model

Setup

The experiment was carried out with an axisymmetric nacelle placed in the NLR low-speed wind tunnel (Fig. 1). This nacelle consists of a duct with a hub, connected by struts at the rear, and a row of equidistant stator vanes farther upstream (Fig. 2). Upstream of the stator, a rotor is mounted, driven by an air motor inside the hub. The diameter of the flow tube is 400 mm, the diameter of the hub is 240 mm, the gap between rotor and stator is 15 mm.

The stator consists of 18 unleaned and unswept vanes aligned with the uniform flow. Their chordwise sections are uncambered NACA 0010-35 wing sections, which have a thickness of 10%. The chord length, which is constant along the span, is 50 mm. Along a chordwise section of one of the stator vanes, 20 miniature transducers are mounted symmetrically at the lower and upper sides. This particular vane is movable in the radial direction, such that measurements can be done at several spanwise positions. Measurements were carried out at three positions: 30% annular span (from the hub), 53% span, and 76% span.

Fig. 1 Fan model in wind tunnel.

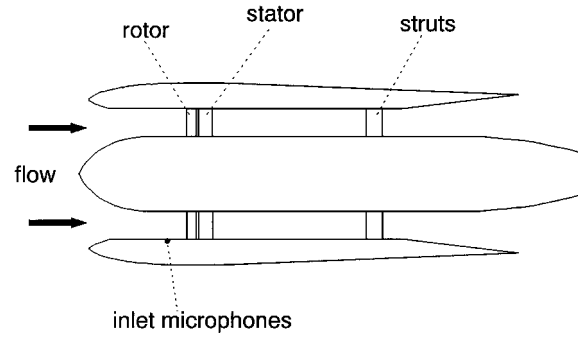

Fig. 2 Schematic drawing of experimental model.

The rotor consists of 16 unleaned and unswept blades. The stagger angles are adjusted such that the incident relative flow angle is zero when the rotor rotates with 6650 rpm and the axial flow is 85 m/s. The blades have a constant axial chord length of 40 mm; hence, the actual chord length varies in the spanwise (radial) direction. The blade section at the hub is a NACA 0010-35 section; at other radii, modified NACA 0010-35 sections are used. The relative thickness of these modified sections is reduced such that the absolute maximum thickness is constant. Also, one of the rotor blades is equipped with transducers, six at each side of the midspan section. Because a rotor blade is not movable without violating the geometry, measurements could be carried out only at this one radius. Furthermore, an annular array of 22 equidistant transducers was installed at the inner wall of the duct, 80 mm upstream from the rotor, to measure the unsteady wall pressures of circumferential modes.

The accuracy of the pressure transducers used in the stator, rotor, and inlet wall is approximately 1 dB (12%). For convenience, some dimensionless coordinates are listed in Table 1.

Trip Wires

During the tests, the axial Mach number was varied from 0.10 to 0.23. As a result, the Reynolds number of the flow along the blades had values between 10^5 and 10^6, a region in which transition from laminar to turbulent boundary-layer flow is very sensitive to the Reynolds number. Therefore, it is possible that the location of the transition varied with time, and the motion of the transition points would affect the generation of sound in an unpredictable manner. To suppress this undesirable effect, which does not occur at the high Reynolds numbers in a full-size turbofan, trip wires were attached at midchord to both sides of the rotor blades and stator vanes.

Table 1 Dimensionless coordinates of experimental setup

Nacelle	Tip radius	$r = 1$
	Hub radius	$h = 0.6$
	Intake tranducers	$x = 0$
Rotor	Blade number	$B = 16$
	Leading edge	$x = 0.400$
	Trailing edge	$x = 0.600$
	Transducers	$r = 0.800$
Stator	Vane number	$V = 18$
	Leading edge	$x = 0.675$
	Trailing edge	$x = 0.925$
	Transducers	$r = 0.720$
		$r = 0.813$
		$r = 0.905$

Conditions

Measurements were carried out at a number of different rotor revolutions per minute. The following nominal revolutions per minute were selected to measure with: 3240, 3865, 4565, 4750, 5440, 5550, 6425, and 7000. Nominal revolutions per minute (rpm_0) is defined as

$$\text{rpm}_0 = \text{rpm} \times \sqrt{T_0/T} \tag{17}$$

where T is the actual temperature and T_0 is the standard temperature (288.16 K). Hence, the tip Mach number Ω of the rotor was chosen in advance, but the actual revolutions per minute depended on the temperature. The Mach numbers of the main flow in the duct were adjusted such that the steady loading of the rotor is as small as possible.

With the present setup and conditions, the rotor and stator have no steady loading, and sound is generated by the viscous wakes from the rotor and by the flow distortion caused by the thickness of the rotor blades and the stator vanes. It is noted that the rotor blades and the stator vanes are much thicker and the rotor–stator gap is much smaller than in an actual turbofan engine, where the influence of blade and vane thickness is negligible.

V. Validation

The aim of the experiment was to validate the lifting surface theory for a rotating blade row (the rotor), using a known incident acoustic field. As mentioned in the Introduction, the unsteady lifting surface theory was already validated for a stator in 1989.[4]

The incident field on the rotor is induced by the unsteady loading and the thickness of the stator vanes. The thickness part of the incident field must be calculated, but for the loading part the measurements could be used. However, we will use calculated stator loading to ensure that the phases of the different contributions to the incident field are in the correct proportion. Because of the small gap between rotor and stator, some adjustment to the calculated stator loading was needed, as will be described next.

Stator

Unsteady stator loading is caused by several types of interaction: interaction with steady and unsteady loading of the rotor blades (acoustic modes as well as vortices), interaction with flow distortions caused by the thickness of the rotor blades, and interaction with viscous wakes. In the present experiment only the latter two make significant contributions.

Drag Coefficients

In the viscous wake model, i.e., Schlichting's turbulent wake model,[9] the drag coefficients of the rotor blade sections are required as input. For high Reynolds numbers ($Re \geq 3 \times 10^6$), the drag coefficient of a smooth NACA 0010-35 section is known from Ref. 11. However, in the experiment the Reynolds numbers are much lower, between 10^5 and 10^6. Moreover, only at the hub is a genuine NACA 0010-35 section used for the rotor blade section. At other radial positions, modified versions of this section are used (see Sec. IV). Furthermore, attached trip wires will affect the drag as well.

To obtain the required drag coefficients, measurements of wake velocities behind wing sections were performed. Two constant chord

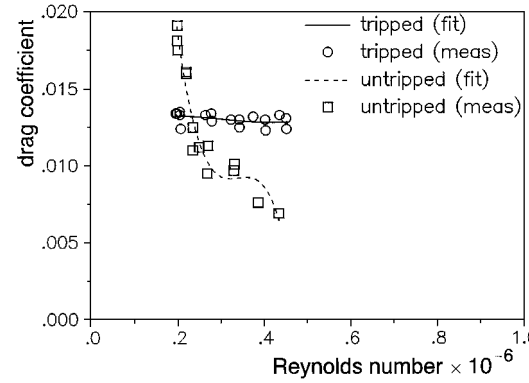

Fig. 3 Drag coefficients of rotor hub section (10% thickness).

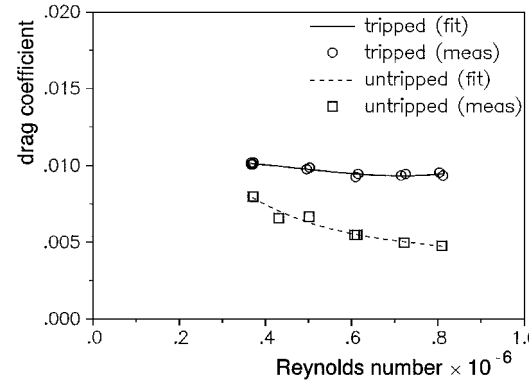

Fig. 4 Drag coefficients of rotor tip section (7% thickness).

models were manufactured especially for this purpose: a 10% thick model, with cross section identical to the stator vane sections and the rotor blade hub sections (NACA 0010-35), and a 7% thick model, with cross section identical to the rotor blade tip sections. The wake measurements were carried out with and without trip wires. The Reynolds number range was the same as in the fan experiment.

The measured drag coefficients, together with least-squares fits, are plotted in Figs. 3 and 4 as a function of the Reynolds number. The measurements show that, for not-too-low Reynolds numbers, tripping the wings causes the drag to increase significantly, up to a factor of 2. The measurements behind the 10% thick model (Fig. 3) demonstrate that the drag of the untripped model is very sensitive to the Reynolds number, in contrast to the drag of the tripped model. This illustrates the benefit of the trip wires, in particular at lower Reynolds numbers occurring at the stator vanes and at the hub sections of the rotor blades. As input for the theoretical model, the least-squares fits (Figs. 3 and 4) of the drag coefficients were used for the sections at the hub and the tip. For sections in between, the drag coefficient has been assumed to vary linearly with the radial coordinate.

Thickness of Rotor Blades

A complication that arises when calculating the unsteady stator loading is caused by the thickness of the rotor blades. The rotor blade sections have a maximum thickness of 10%, considerably thicker than commonly used in turbofans. This blade thickness was needed to accommodate the pressure transducers. However, it is too thick to carelessly apply linearized theory for calculating the induced disturbance velocity. Because of the boundary layer, the effective thickness is even more than 10%. Linearized theory, which models the blade thickness by velocity monopoles on the reference surfaces, tends to underpredict the actual distortion for such thick blades. (This can be verified by sample calculations of two-dimensional potential flow around Joukowski airfoils.[12])

In the experiment, the gap between rotor and stator is much smaller than usual, and as a result the thickness of the rotor blades plays an important role in the first harmonic stator loading (BPF). For higher harmonics, the influence of rotor blade thickness rapidly vanishes.

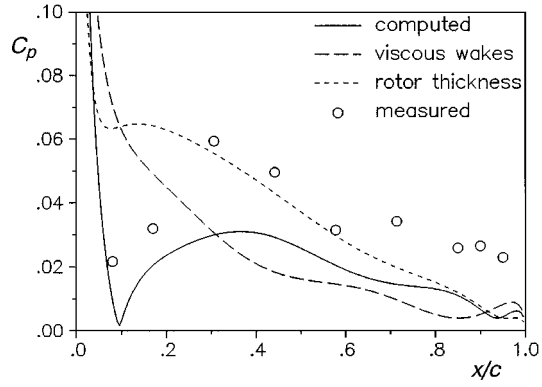

Fig. 5 Stator unsteady pressure, 5550 rpm$_0$, modulus of pressure jump at $r = 0.8125$, first harmonic.

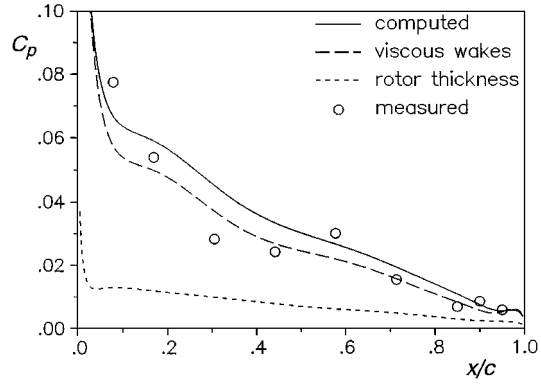

Fig. 6 Same conditions as Fig. 5, second harmonic.

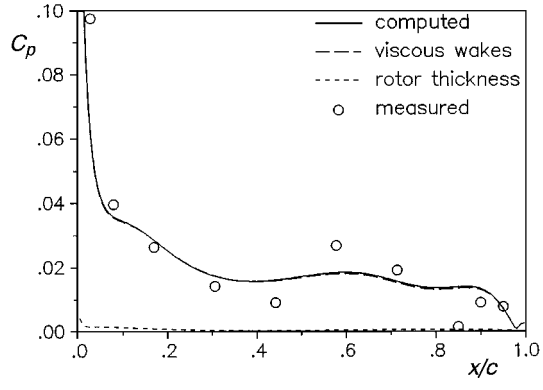

Fig. 7 Same conditions as Fig. 5, third harmonic.

In Figs. 5–7, results are shown for the first three harmonics at $r = 0.813$ of the unsteady stator loading for the case of 5550 rpm$_0$. The computed as well as the measured moduli of the pressure jumps are plotted. Moreover, the (computed) contributions of rotor blade thickness and viscous wakes are shown. It is noted that the two contributions are in counterphase in the first harmonic and in phase for the second harmonic. In the third harmonic the influence of rotor thickness is negligible. The computed results at the first harmonic (Fig. 5) are significantly lower than the measured results. The reason for this discrepancy is probably that the theory underpredicts the contribution of the rotor blade thickness. If this contribution is multiplied with a nonlinearity factor of 1.4, a much better agreement is found (see Fig. 8). For higher harmonics (Figs. 6 and 7), such a multiplication does not affect the good agreement.

The same procedure, i.e., multiplying the contribution of rotor thickness in the first harmonic of the stator loading with 1.4, is followed for other nominal revolutions per minute. In each case and for each harmonic, good agreement is found. Thus, the obtained unsteady stator pressures are used as input for the unsteady rotor calculations.

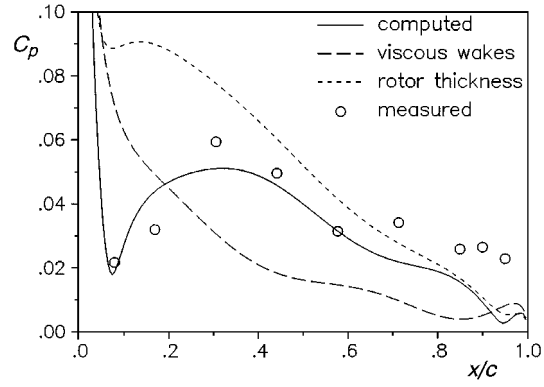

Fig. 8 Same conditions as Fig. 5, calculated with nonlinear correction.

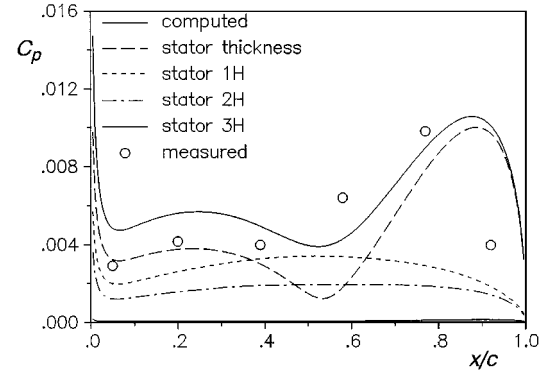

Fig. 9 Rotor unsteady pressure, 5550 rpm$_0$, modulus of pressure jump at midspan, first harmonic.

Rotor

The unsteady pressure on the rotor blades is induced by incident acoustic modes, radiating from the stator, with frequencies $\omega_k = n_1 \times 16\Omega$ and mode numbers $k = n_1 \times 16 - n_2 \times 18$ (see Sec. II). The induced unsteady rotor blade loading consists of frequencies $\omega_l = n_2 \times 18\Omega$, multiples of the stator-vane-passing frequency. It is noted that each harmonic n_1 on the stator contributes to each harmonic n_2 on the rotor.

For the rotor first and second harmonics ($n_2 = 1, 2$), which are the cases considered in the validation, it appears that only the stator first, second, and third harmonics ($n_1 = 1, 2, 3$) contribute significantly. Higher harmonics ($n_1 > 3$) and steady loading ($n_1 = 0$) on the stator have negligible influence.

Another contribution to the unsteady loading of the rotor blades is the (steady) flow distortion caused by the thickness of the stator vanes. This field can be decomposed into acoustic modes of zero frequency, $\omega_k = 0$, and mode numbers $k = -n_2 \times 18$. Again, the corresponding frequencies at the rotor blades are given by $\omega_l = n_2 \times 18\Omega$.

In Fig. 9 the computed and measured first harmonic unsteady rotor loadings at 5550 rpm$_0$ are plotted. Also the several components that contribute to the total loading are plotted. In Fig. 10 similar results are plotted for the second harmonic. It is seen that, though it is a complicated process to compute the total loading in which several contributions are of the same order of magnitude, the agreement with the measurements is good.

In Figs. 11 and 12 the measured and computed, first and second harmonics of the rotor loading are plotted for two other nominal revolutions per minute: 3240 and 6425. This is done without showing the several components by which it is built up. In both cases, the agreement between theory and experiment is good.

Inlet

Three source mechanisms contributing to the resulting acoustic pressure in the duct inlet can be distinguished. First, from the stator, acoustic modes emanate with frequencies $\omega_k = n_1 \times 16\Omega$ and mode numbers $k = n_1 \times 16 - n_2 \times 18$. Second, by interaction with the

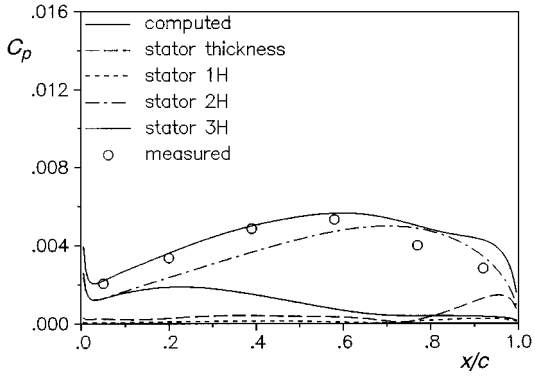

Fig. 10 Same conditions as Fig. 9, second harmonic.

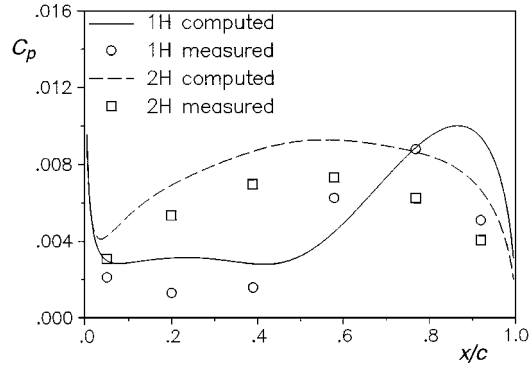

Fig. 11 Rotor unsteady pressure, 3240 rpm_0, modulus of pressure jump at midspan, first and second harmonics.

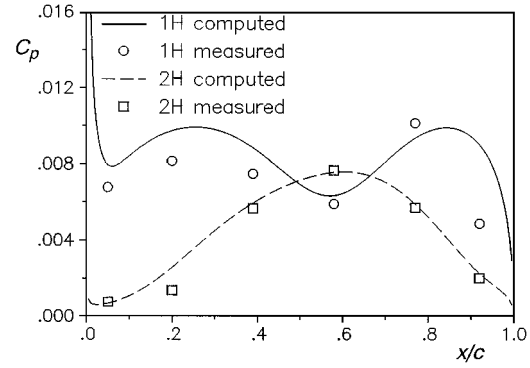

Fig. 12 Rotor unsteady pressure, 6425 rpm_0, modulus of pressure jump at midspan, first and second harmonics.

rotor, modes arise with frequencies $\omega_k = (n_1 + n_3) \times 16\Omega$ and mode numbers $k = (n_1 + n_3) \times 16 - n_2 \times 18$. The third contribution is the interaction of the rotor with the disturbance velocity induced by the thickness of the stator vanes, yielding an acoustic field with frequencies $\omega_k = n_3 \times 16\Omega$ and mode numbers $k = n_3 \times 16 - n_2 \times 18$.

In each case, acoustic modes appear with frequencies $\omega_k = n \times 16\Omega$ and mode numbers $k = n \times 16 - n_2 \times 18$, in accordance with the theory of Ref. 1. At BPF ($n = 1$), the only radial cuton mode in the considered frequency range is the mode with the lowest circumferential mode number, that is, $k = -2$, obtained with $n_2 = 1$. At $2 \times$ BPF ($n = 2$), the only cuton mode is $k = -4$, obtained with $n_2 = 2$.

To illustrate the importance of the several sources, we consider again the case of 5550 rpm_0. The pressure amplitude at BPF (with $k = -2$), computed at the inlet wall, is a summation of several contributions with the following amplitudes: direct radiation from the stator, 11.8 Pa; interaction of rotor with stator thickness, 13.9 Pa; interaction of rotor with stator first harmonic, 14.8 Pa; interaction of rotor with stator second harmonic, 5.5 Pa; and interaction of rotor with stator third harmonic, 0.2 Pa. Summation of these contributions, each with its own phase, yields a pressure amplitude of 21.2 Pa. The measured counterpart in this case was 21.7 Pa. Thus, the computed and the measured inlet pressure amplitudes are remarkably close to each other. On a decibel scale the difference is only 0.2 dB, which is within the accuracy of the measurements.

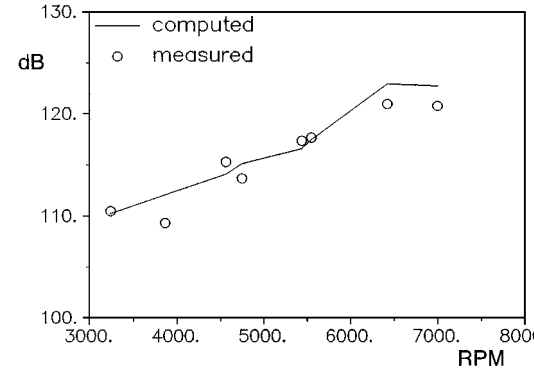

Fig. 13 Inlet SPL at BPF, $k = -2$.

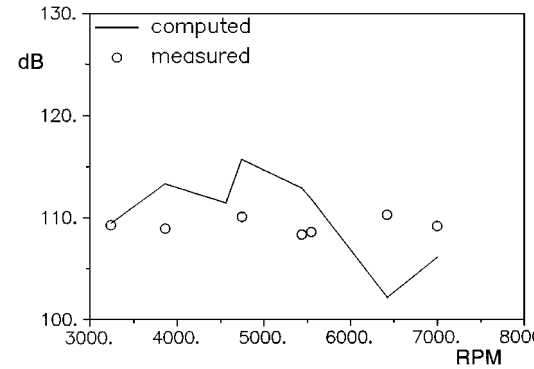

Fig. 14 Inlet SPL at $2 \times$ BPF, $k = -4$.

For the entire range of nominal revolutions per minute, the sound pressure levels (SPL) of the computed and measured inlet wall pressures at BPF (with $k = -2$) are plotted in Fig. 13. The difference between numerical and experimental results is within 3 dB. The largest differences are observed at the lowest nominal revolutions per minute. This is probably due to inlet reflections, which are nonnegligible at frequencies close to cutoff (BPF is cut off at 2550 rpm_0). Inlet reflections are not included in the present calculations. For the high nominal revolutions per minute, where the weakest inlet reflections are expected, the results are within 2 dB.

In Fig. 14, computed and measured SPLs are plotted for $2 \times$ BPF (with $k = -4$). The extremely low measured result for 4565 rpm_0 falls outside of the range of the figure: 83 dB. The agreement is less good than at BPF. The poor agreement is in contrast to the good agreement of the first and second harmonic unsteady loading at rotor and stator. Inlet reflections may partly account for the differences between theory and measurement but do not explain the extremely low measured value at 4565 rpm_0. It is remarked here that mode scattering cannot be a cause for the discrepancies because hardly any mode scattering was observed.

VI. Conclusions

A wind-tunnel experiment has been carried out with a fan model designed to study rotor–stator interaction noise. Because the Reynolds numbers were lower than for a typical turbofan stage, trip wires were attached to rotor blades and stator vanes to fix the point of transition from laminar to turbulent boundary flow. The aim of the experiment was the validation of a lifting surface theory for a rotating blade row.

For a range of revolutions per minute, the unsteady loading was measured on a rotor blade and the first and the second harmonics were compared with theoretical results. Good agreement was found.

Furthermore, inlet wall pressure measurements were compared with results from the theory. At BPF the agreement is good. Small differences at lower revolutions per minute can be explained by inlet

reflections. For conditions where the inlet reflection is expected to be weak, theoretical and experimental results are within 2 dB. For $2 \times$BPF, however, the agreement is poor, which cannot entirely be explained by reflections.

For a more comprehensive validation, it seems necessary to include acoustic inlet and outlet reflections in the theoretical modeling. In addition, it is advisable to use an experimental model with higher Reynolds numbers, a larger separation of rotor and stator, and thinner blade sections.

Acknowledgment

This research was supported by the Netherlands Agency for Aerospace Programs NIVR, Contract 01402N.

References

[1]Tyler, J. M., and Sofrin, T. G., "Axial Flow Compressor Noise Studies," *SAE Transactions*, Vol. 70, 1962, pp. 309–332.

[2]Schulten, J. B. H. M., "Sound Generation by Ducted Fans and Propellers as a Lifting Surface Problem," Ph.D. Thesis, Dept. of Applied Mathematics, Univ. of Twente, Enschede, The Netherlands, Feb. 1993.

[3]Schulten, J. B. H. M., "Transmission of Sound Through a Rotor," *Proceedings of the DGLR/AIAA 14th Aeroacoustics Conference* (Aachen, Germany), Vol. 1, Deutsche Gesellschaft für Luft- und Raumfahrt, Bonn, Germany, 1992, pp. 502–509.

[4]Schulten, J. B. H. M., "Experimental Validation of a Lifting Surface Model for Rotor Wake–Stator Interaction," AIAA Paper 89-1125, April 1989.

[5]Zandbergen, T., "Stator Vane Response due to the Impingement of the Wake of an Unloaded Rotor," AIAA Paper 88-2814, July 1988.

[6]Fleeter, S., Jay, R. L., and Bennett, W. A., "Rotor Wake Generated Unsteady Aerodynamic Response of a Compressed Stator," *Journal of Engineering for Power*, Vol. 100, Oct. 1978, pp. 664–675.

[7]Fleeter, S., "Fluctuating Lift and Moment Coefficients for Cascaded Airfoils in a Nonuniform Compressible Flow," *Journal of Aircraft*, Vol. 10, No. 2, 1973, pp. 93–98.

[8]Tam, C. K. W., and Webb, J. C., "Dispersion-Relation-Preserving Finite Difference Schemes for Computational Acoustics," *Journal of Computational Physics*, Vol. 107, No. 2, 1993, pp. 262–281.

[9]Schlichting, H., *Boundary Layer Theory*, McGraw–Hill, New York, 1979, Chap. 24.

[10]Schulten, J. B. H. M., "Vane Sweep Effects on Rotor/Stator Interaction Noise," *AIAA Journal*, Vol. 35, No. 6, 1997, pp. 945–951.

[11]Abbot, I. H., and von Doenhoff, A. E., *Theory of Wing Sections*, Dover, New York, 1959, p. 459.

[12]Batchelor, G. K., *An Introduction to Fluid Dynamics*, Cambridge Univ. Press, London, 1967, pp. 444–449.

R. W. Wlezien
Associate Editor